# Silicon photonics traveling wave photodiode with integrated star coupler for high-linearity mm-wave applications

LAURENS BOGAERT,[1,2,*] KASPER VAN GASSE,[1] THIJS SPUESENS,[1] GUY TORFS,[2] JOHAN BAUWELINCK,[2] AND GUNTHER ROELKENS[1]

[1]*Photonics Research Group, Dep. INTEC, Ghent University–Imec, Technologiepark-Zwijnaarde 15, B-9052 Ghent, Belgium*
[2]*IDLab, Dep. INTEC, Ghent University–Imec, Technologiepark-Zwijnaarde 15, B-9052 Ghent, Belgium*
**laurens.bogaert@ugent.be*

**Abstract:** Next-generation wireless communication will require increasingly faster data links. To achieve those higher data rates, the shift towards mmWave frequencies and smaller cell sizes will play a major role. Radio-over-Fiber has been proposed as a possible architecture to allow for this shift but is nowadays typically implemented digitally, as CPRI (Common Public Radio Interface). Centralization will be important to keep next-generation architectures cost-effective and therefore shared optical amplification at the central office could be preferable. Unfortunately, limited power handling capabilities of photodetectors still hinder the shift towards centralized optical amplification. Traveling wave photodetectors (TWPDs) have been devised to allow for high-linearity, high-speed opto-electronic conversion. In this paper, an architecture is discussed consisting of such a TWPD implemented on the iSiPP25G silicon photonics platform. A monolithically integrated star coupler is added in the design to provide compact power distribution while preserving the high linearity of the TWPD. The traveling wave structure (using 16 photodetectors) has a measured 3 dB bandwidth of 27.5 GHz and a fairly flat $S_{21}$ up to 50 GHz (less than 1 dB extra loss). Furthermore, the output referred third-order intercept point at 28 GHz, is improved from -1.79 dBm for a single Ge photodiode to 20.98 dBm by adopting the traveling wave design.



## 1. Introduction

Future wireless communication links will require increasingly higher data rates to accommodate next generation applications [1]. Densification of communication cells will play a major role in the shift towards faster wireless data rates. To keep this technique economically and ecologically viable, a centralized approach needs to be pursued. A second key enabler for higher data rates is the usage of different parts of the spectrum. Millimeter wave (mmWave) frequencies are of great interest since they offer larger bandwidths and they are significantly less congested. Different schemes have been devised to enable centralization for mmWave communication. For instance Analog Radio-over-Fiber (ARoF) is a straightforward implementation where the RF signal is generated at the central office (CO), modulated on an optical carrier, and subsequently transmitted to the desired remote antenna unit (RAU) [2]. After transmitting the signal from the CO to the RAU, an opto-electronic conversion is performed by a photodetector. This RF signal should then be amplified such that it is sufficiently strong to overcome path losses in the wireless channel between the RAU and the end user. This is typically done by adding a transimpedance amplifier (TIA) followed by a power amplifier [3-4]. The aforementioned architecture can be altered to a more centralized topology by moving the amplifiers to the optical domain, where the amplification can be done for multiple RAUs at once, resulting in a significant decrease in RAU complexity

and power consumption. However, the linearity of a high-speed photodetector (PD) is typically inadequate to allow for high RF output power [5]. Improving the power handling capabilities of the photodetectors eventually allows for the omission of electrical amplification in the DL-RAU (downlink RAU, i.e. from central office to mobile end user), paving the road for passive DL-RAUs [6]. Implementing such high-power-handling photodiodes on a silicon photonics platform enables the low-cost manufacturing of such devices in high volume. Moreover, it also allows the integration of other optical functionality (e.g. an optical beam forming network) on the same circuit. To improve the power handling capabilities of an integrated high-speed p-i-n photodetector one can opt to use different materials and detector principles (e.g. III-V uni-travelling carrier photodetectors integrated on silicon [7-13]) or more complex photodetector configurations. While UTC photodetectors are often being used as high-power, high-speed photodetectors, they are not CMOS compatible because of their complex layer stack based on III-V materials (typically InGaAs-InP). To make optimal use of the aforementioned benefits of silicon photonics, a high-power variant of the existing Si-integrated Ge PiN photodetector needs to be constructed without altering the technology stack of the iSiPP25G platform or requiring heterogeneous integration. The traveling wave photodiode (TWPD) structure is the most popular configuration to realize high power handling while relying on high-speed p-i-n photodetectors [14]. In this paper, a high-power-handling traveling wave photodetector (TWPD) structure integrated on a silicon photonics waveguide platform will be discussed. The traveling wave structure (using 16 photodetectors) has a measured 3 dB bandwidth of 27.5 GHz and has a fairly flat $S_{21}$ up to 50 GHz (less than 1 dB extra loss). Furthermore, the output referred IP3 linearity at 28 GHz is improved from -1.79 dBm for a single Ge photodiode to 20.98 dBm by adopting a traveling wave design with dual-fed photodetectors.

## 2. Ge traveling wave photodetectors on a Si photonics platform

In this work, the iSiPP25G silicon photonics platform of imec is used to realize the traveling wave photodetector structure. The germanium photodiodes available on the platform have a responsivity of 0.8 A/W and a bandwidth of more than 50 GHz. However, their power handling capabilities are limited, as will be discussed below. A clever rearrangement of the photodetector structure and splitting the power over multiple PDs can significantly increase the linearity.

### *2.1 Dual fed photodetectors*

While the standard mode of operation for the Ge photodiode on the iSiPP25G platform is to use a single optical input waveguide, one of the features available in the platform is that the Ge PDs can be optically fed from two sides. This immediately allows for a linearity improvement by increasing the optical input power for which compression occurs in the optoelectronic conversion. By adding a splitter in front of the PD, the linearity can be improved at the cost of a slight increase in insertion loss (due to the excess loss of the splitter, which is specified to be below 0.2 dB). This enhanced power handling capability is caused by the increased portion of the absorption layer that is used for the opto-electronic conversion [14].

### *2.2 Increasing the number of photodetectors*

Another solution to improve the power handling capability of the optoelectronic conversion is to increase the number of photodetectors per RAU. The power handled per individual PD drops proportional with the amount of PDs, enhancing the power limit of the RAU significantly. However, in the electrical domain the RF signals will need to be recombined constructively.

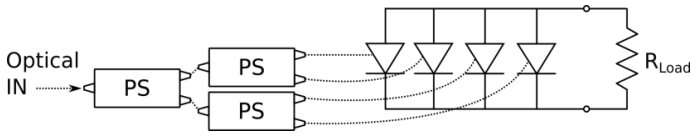


Fig. 1. Lumped parallel PD configuration (PS: Power Splitter, $R_{Load}$: Load Resistor).

Combining multiple PDs in a lumped parallel fashion, as shown in Fig. 1, results in a linearity improvement but gravely deteriorates the bandwidth of the PD because of the increased capacitance forming a low pass RC filter. Adopting a traveling wave configuration to recombine the electrical signals originating from the individual PDs allows for high-speed, high-linearity opto-electronic conversion. The underlying idea is that the PD parasitics are embedded in a transmission line design and therefore do not result in RC filtering.

### *2.3 Proposed traveling wave architecture*

In Fig. 2, the proposed high-power handling photodetector architecture is depicted together with a 16-PD implementation in the iSiPP25G silicon photonics platform. The design consists of three major parts. Firstly, a TWPD is used to allow for high-linearity, high-speed opto-electronic conversion. As discussed before, each PD will be dual fed to enhance the linearity of each Ge PD individually. Secondly, the goal is to recombine the RF signal from the individual Ge PDs constructively in the load. This will be accomplished by matching the optical and electrical delay using optical delay lines. Electrical signals originating from PDs closer to the load experience a smaller delay because of a shorter propagation distance along the transmission line. Hence, this should be compensated for in the optical domain to make sure that the different portions of the signal arising from the different PDs arrive simultaneously at the load. Lastly, incident power needs to be distributed among the PDs. Typical implementations use power splitting trees based on multiple 3 dB splitters [14]. In this paper, a monolithically integrated star coupler is used instead. This allows for improving the power handling capabilities of the passive waveguide circuit, which is limited by two-photon absorption [15]. The presence of a star coupler instead of a power splitting tree will become even more important when the number of photodiodes in a traveling wave photodiode is increased to further improve the linearity of the optoelectronic conversion and eventually enable a passive DL-RAU.

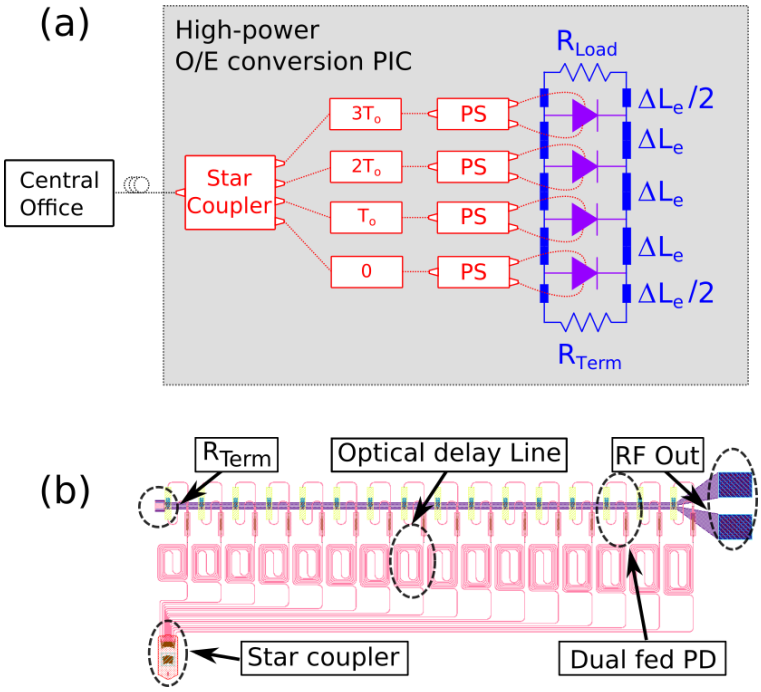


Fig. 2. Germanium traveling wave photodetector structure: (a) schematic; (b) layout of the fabricated device (PS: Power Splitter, $T_o$: Optical Delay, $\Delta L_e$: transmission line segment length).

### *2.4 Traveling wave photodiode design and simulation results*

In this section, the TWPD will be discussed in greater detail. The main goal of the opto-electronic conversion is to provide an as large as possible power to the load impedance $R_{Load}$. This load impedance describes the input impedance of the antenna. To get an optimal power transfer from the TWPD to the load, three criteria need to be fulfilled [14]. Firstly, delays in the optical and electrical domain should be matched. This is done by adding optical delay lines, as discussed before. Secondly, the characteristic impedance of the loaded transmission line should be sized in such a way that no reflections occur at the interface between the TWPD and the load. A final important part of the TWPD design is the presence of a termination resistor $R_{Term}$ at the opposite side of the TWPD. This termination absorbs backwards propagating waves. If $R_{Term}$ is omitted, backwards propagating waves will couple to the forward direction resulting in interference and an associated bandwidth reduction.

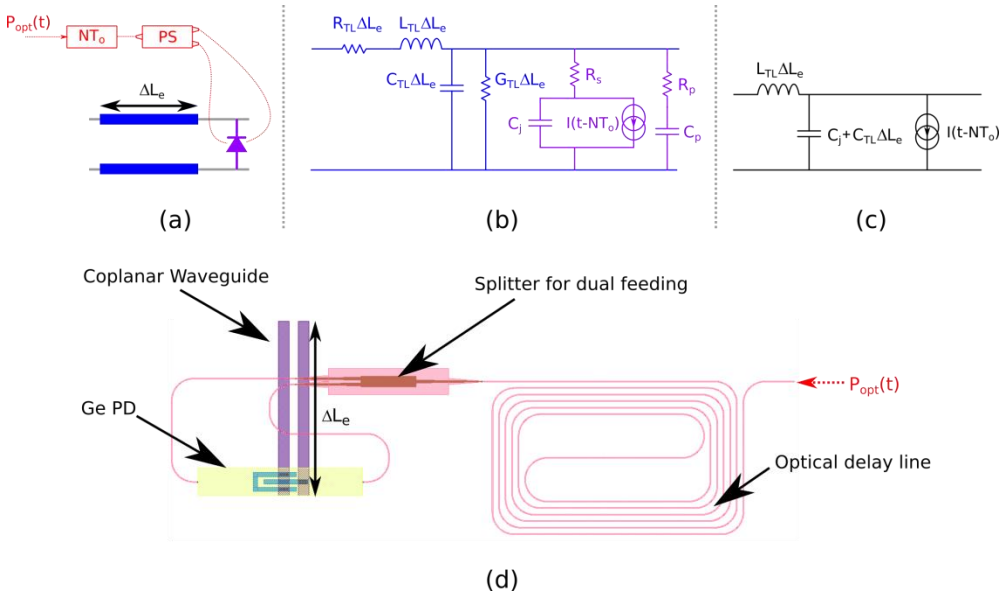


Fig. 3. TWPD model for a single photodetector-loaded transmission line segment (a) one segment; (b) its equivalent model; (c) a lossless equivalent model; (d) the layout of one fabricated segment.

A first step in the design of the TWPD consists of constructing a suitable distributed model for the transmission line periodically loaded with discrete photodetectors. The adopted model is shown in Fig. 3. In the initial sizing, losses were ignored to enable the usage of simplified design formulas. $L_{TL}$, $C_{TL}$, $R_{TL}$ and $G_{TL}$ are the per unit length parameters of the unloaded transmission line itself while $C_j$, $R_s$, $R_p$ and $C_p$ are part of the photodetector model ($C_j$ is the junction capacitance, $R_s$ the series resistance, and $R_p$ and $C_p$ describe the coupling to the substrate). The constructed equivalent model for the photodetector is based on S-parameter measurements, which were performed on nominally identical photodiodes as used in our traveling wave photodiode structure, under a range of reverse voltages. For the adopted photodetector at a 2V reverse biasing, the following mean values for $R_s$, $C_j$, $R_p$ and $C_p$ were found: $R_s \cong 35$ Ohm, $C_j \cong 35$ fF, $R_p \cong 1250$ Ohm and $C_p \cong 100$ fF. The simplified model depicted in Fig. 3(c) provides guidelines [16] for impedance matching and delay matching and those guidelines are respectively given in Eqs. (1) and (2).

$$R_{Term} = R_{Load} = \sqrt{\frac{L_{TL}}{C_{TL} + C_j/\Delta L_e}} \tag{1}$$

$$T_o = \frac{\Delta L_e}{v_e} = \frac{\Delta L_o}{v_{o,g}} \tag{2}$$

The delay matching criterion consists of the electrical delay length $\Delta L_e$, the velocity of the RF signal $v_e$, the optical delay length $\Delta L_o$, and the group velocity of the optical signal $v_{o,g}$ . The velocity of the electrical and optical signal can be found from Eqs. (3) and (4).

$$\frac{1}{v_e} = \sqrt{L_{TL}(C_{TL} + C_j/\Delta L_e)} \tag{3}$$

$$v_{o,g} = \frac{c}{n_g} = \frac{c}{4.26} \tag{4}$$

In Eq. (4), the constant c denotes the speed of light and $n_g$ is the group index which is 4.26 at 1550 nm for the 450 nm wide waveguides used in the delay line. The TWPD was designed in the iSiPP25G platform starting from Eq. (1), with a target load impedance of 50 Ohm. The Ge photodetector used for the designed TWPD has a 35 fF junction capacitance at 2V reverse biasing. Taking into account these parameters and the requirements on minimal trace width (imposed by design rules and the heating of the traces) and minimal trace spacing (imposed by design rules), the coplanar waveguide shown in Fig. 3(d) was designed (with trace widths of 5 µm and a gap of 4.2 µm) and periodically loaded with the Ge photodetectors. Subsequently, the delays were matched by designing an optical delay line based on Eq. (2). For the demonstrated device, a 35.4 Ohm characteristic impedance of the TWPD was obtained. This number was obtained by re-simulating the device with the fabricated dimensioning. The deviation relative to the targeted 50 Ohm characteristic impedance can be attributed to the fact that the PD spacing ΔLe was chosen too small (80 µm instead of the desired 190 µm). The designed TWPD segment is depicted in Fig. 3(d) and the entire TWPD is shown in Fig. 2(b).

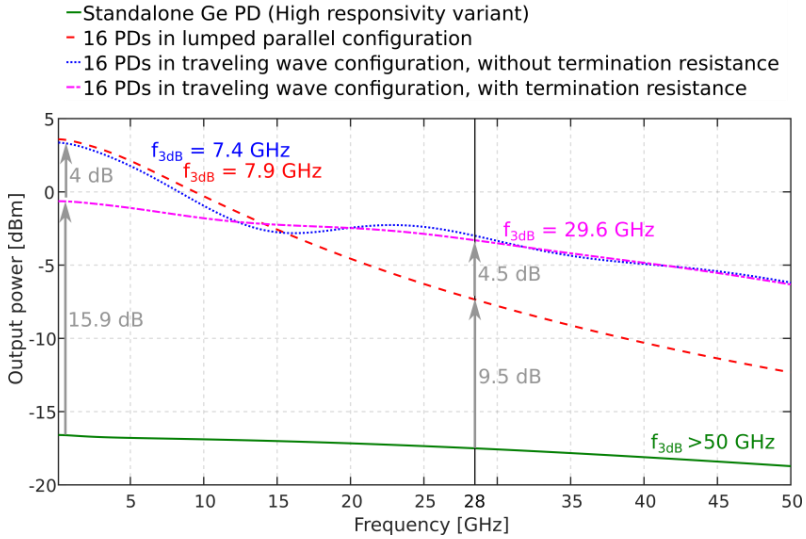


Fig. 4. Simulated output power in a 50 Ohm load for the different structures when each PD individually generates 2 mA peak-to-peak current (2V reverse voltage, 50 Ohm termination).

The simulated frequency dependent behavior of the different structures is given in Fig. 4. These simulations are performed with the dimensions adopted in the fabricated device (hence the TWPD has a characteristic impedance of 35.4 Ohm). Simulations on the terminated TWPD show that only a 0.8 GHz increase in 3-dB bandwidth can be expected when the device is adapted such that the correct dimensions are being used. The most important difference between the fabricated and the ideally dimensioned device is that even for the terminated TWPD some minor interference effects can be observed when the sizing is erroneous. This is due to the non-perfectly matched impedance levels in the fabricated TWPD. When a multi-PD structure is used, the low frequency current sunk into the load is expected to scale with the number of PDs and therefore the available power at the load is following a quadratic scaling with the PD count if the current per photodetector remains the same. Since the implemented multi-PD structures consist of 16 photodetectors, the low

frequency output power should increase with 24 dB when the current per photodetector is kept constant. Additionally, since a termination resistor absorbs the backwards propagating waves in a transmission line, a 6 dB drop at low frequencies is expected when adding a termination to the TWPD. In practice, however, additional substrate losses will reduce the power gain. These substrate losses are modeled by $R_p$ in Fig. 3(b) and its resistance value is found to be close to 1250 Ohm for the given photodetector. For the unterminated TWPD, they reduce the ideal power gain by 4.1 dB, resulting in 19.9 dB gain compared to the standalone PD. The terminated TWPD only sees 2.1 dB of power loss introduced by the presence of substrate losses. This results in a 15.9 dB power gain compared to the standalone PD rather than the 18 dB gain that would be achieved in the absence of any substrate losses. Secondly, Fig. 4 indicates that at higher frequencies there is little to no difference between the TWPD with and without termination resistor. This can be attributed to the lossy nature of the transmission line attenuating back-traveling reflections that interfere with the normal traveling wave operation, consequently resulting in damped interference effects at higher frequencies. It appears that the transmission line losses are mainly caused by the high series resistance $R_s$ of the photodetector, which is 35 Ohm for the used photodetector structure and should be as close to zero as possible for an ideal TWPD. When this series resistor is omitted in simulations, interference peaks and dips are clearly visible even at higher frequencies. Comparing the traveling wave configurations with the parallel configuration, it can be seen that the TWPD structure has the potential to provide a significant improvement in bandwidth over the parallel combination of the photodetectors. However, this no longer holds when the dummy termination is omitted. Interference effects between forward propagating waves and reflected backwards propagating waves will result in a major drop in bandwidth. A major drawback however of the presence of a dummy termination is that it inherently results in a power drop, which appears to be a 4 dB drop as shown in Fig. 4.

### *2.5 Star coupler*

The star coupler which was added to our design has been presented in [15]. It adds an integrated 16-way power splitter to a fiber grating coupler from the iSiPP technology platform. Consequently, the incoming light is split immediately over 16 channels and two-photon absorption resulting in non-linear losses is limited because the optical power present in the on-chip waveguides is significantly lowered. For the implemented TWPD, the balanced variant of the star coupler is being used as this provides a power imbalance of only 1.11 dB between the different channels. In [15], up to 275 mW - or equivalently 24.4 dBm - of optical input power was injected in the star coupler without significant non-linear losses.

## 3. Bandwidth measurements

In this section, the different variants of silicon photonics multi-PD structures will be compared in terms of frequency dependence. The lumped parallel combination, given in Fig. 1, will be compared with the traveling wave approach which is shown in Fig. 2. For the latter, the effect of omitting the termination resistor will be studied. Measurement results of the standalone Ge PD are added as a reference.

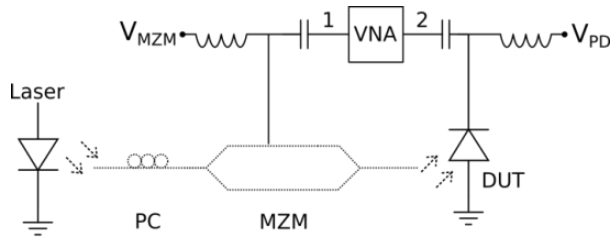


Fig. 5. Setup used for bandwidth measurements (PC: Polarization Controller, MZM: Mach-Zehnder Modulator, DUT: Device Under Test, VNA: Vector Network Analyzer).

The setup depicted in Fig. 5 was used to perform the bandwidth measurements. All measurements were done at a wavelength of 1550 nm. The MZM was biased at its quadrature point and to compensate for the frequency dependent effects in the MZM, a high-bandwidth reference PD was used for calibration. The $S_{21}$ of the link was measured where the DUT was replaced with this reference photodetector and the frequency dependent behavior of this link is assumed to be determined by the transmitter. In subsequent measurements with other DUTs this $S_{21}$ was than subtracted from the measured $S_{21}$ to find the $S_{21}$ of the DUT.

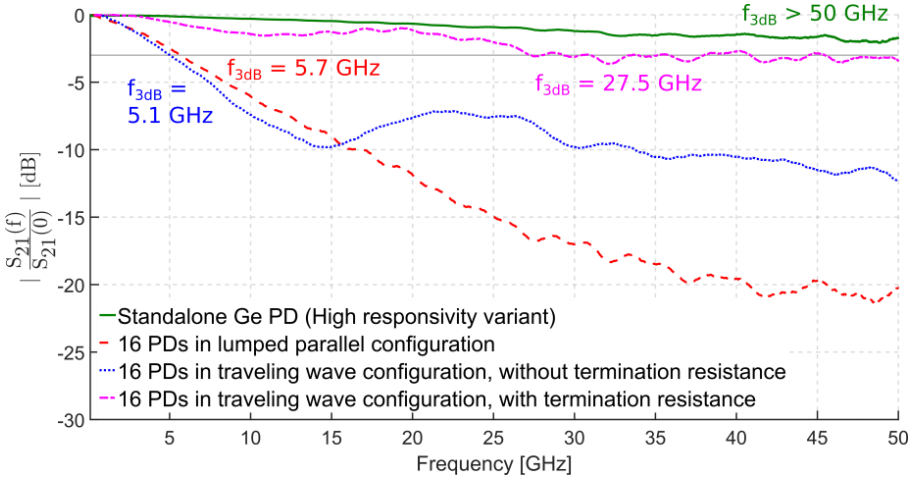


Fig. 6. Measured $S_{21}$ after calibrating out the MZM response.

The different devices are compared in Fig. 6. All DUTs are reverse biased with -2 V. Unlike Fig. 4, the curves are normalized relative to their low frequency value to disregard the differences in coupling losses from the fiber probe to the DUT, which depends heavily on the exact alignment. Fig. 6 shows the high-bandwidth potential of the TWPD structure with dummy termination, while interference notches and peaks are present for the TWPD where the termination resistor is omitted. In the constructed design the termination resistor has a nominal resistance of 50 Ohm at low voltages and the effective resistance value increases up to 64.5 Ohm for 2V reverse biasing due to self-heating of the resistor. At high frequencies, the interference effects become less prominent, as discussed in the previous section. The fact remains that omitting the dummy termination even reduces the bandwidth compared to the straightforward parallel combination of the 16 PDs. The obtained results from Fig. 6 resemble the simulated data from Fig. 4 well, but the bandwidth is slightly less for the measured devices compared to the values obtained in simulations. This can be attributed to an underestimation of the junction capacitance $C_j$ of the photodetector.

## 4. Linearity measurements

In this section, the linearity enhancement obtained from adopting a multi-PD solution is discussed. For all DUTs realized in this work a 2V reverse biasing was used.

### *4.1 DC linearity*

The first linearity measurement that was performed concerns the conversion from CW optical power (at 1550 nm) to DC electrical current by the DUT. The setup used for this

measurement is described in Fig. 7 and the obtained results are provided in Table 1. The EDFA used in this setup is a booster EDFA with tunable output power.

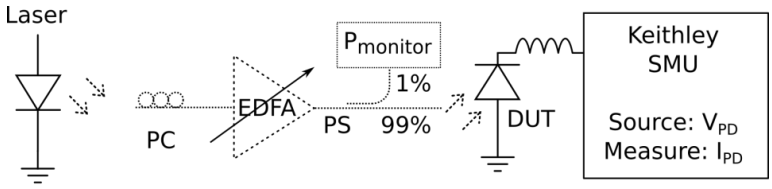


Fig. 7. Setup used for DC linearity measurements (EDFA: Erbium Doped Fiber Amplifier, SMU: source measure unit).

Important to notice when observing the results denoted in Table 1 is that dual feeding indeed provides a higher linearity and that multi-PD solutions offer a substantial increase in power handling capabilities at DC. For the multi-PD solutions, lower boundaries are provided since these structures are still linear at maximum available power (approximately 28 dBm at the fiber probe). The available power at the photodetectors is limited however by coupling losses from the fiber probe to the output of the on-chip grating coupler [15], which is typically between 3 and 7 dB depending on the exact coupling conditions. Hence, the power coupled to the chip is between 125 mW and 316 mW. This will give rise to a photocurrent which is typically between 100 mA and 253 mA (Responsivity ≈ 0.8 A/W) and it is expected that the values given in Table 1 are at the lower side of this range since manual alignment is used. Additionally, the expected current range does not take excess losses into account. The main excess losses present in the system are on the one hand the optical losses caused by the MMIs needed for the dual fed operation (<0.2 dB / MMI) and the waveguide losses in the optical delay lines (approximately 0.26 to 0.41 dB for the different delay lengths) and on the other hand resistive losses in the transmission line (0.05 dB per segment). As the coupling is not the same for the different DUTs due to the alignment of the fiber probe relative to the grating coupler, it is difficult to make a one-to-one comparison of the DC linearity of the multi-PD structures.

**Table 1. 1dB compression current (DC).**

| *Imec iSiPP25G, Silicon Photonics* | |
|---|---|
| Ge PD, Single fed | 8 mA |
| Ge PD, Dual fed | 13.9 mA |
| Lumped parallel configuration, 16 Ge PDs | > 137.4 mA |
| TWPD, 16 Ge PDs, without $R_{Term}$ | > 103 mA |
| TWPD, 16 Ge PDs, with $R_{Term}$ | > 91.8 mA |

For the TWPD with termination resistor, the output current consists of two contributions, as discussed in Fig. 8 (illustrated using a structure consisting of 4 photodetectors). In the absence of light at the input of the device, the structure produces an output current which is proportional to the applied reverse bias voltage. Secondly, a current proportional to the optical input power is generated in the photodetector (with proportionality factor R, the responsivity). The former contribution is subtracted from the measured current to examine the linearity of the opto-electronic conversion. The value provided in Table 1 only considers this opto-electronic contribution.

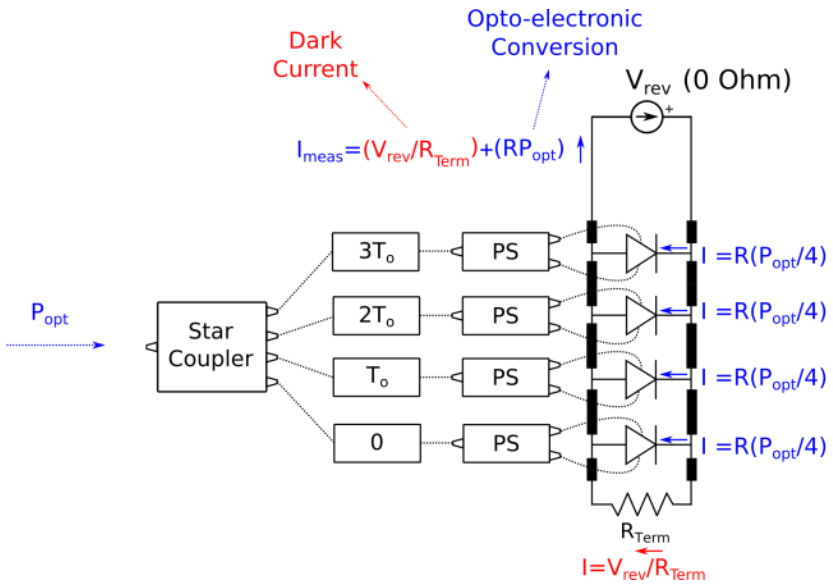


Fig. 8. Current contributions in a terminated TWPD ($P_{opt}$: Optical input power; R: responsivity).

For the 16-PD arrays we expect approximately a 16-fold increase in maximum linear output current, namely 222.4 mA. Unlike for the RF behavior, no coupling to the substrate occurs because of blockage by the buried oxide and hence no drop compared to this 16-fold increase is introduced by the $R_p$. Contrary to the RF measurements, the current was quantified with a low-ohmic load (a Keithley source meter) and therefore the termination impedance does not sink half the current. In the RF measurements, the ESA is a 50 Ohm load and hence, for those measurements, the presence of the termination impedance does not only alter the bandwidth but also the output power.

### *4.2 IP3 measurements*

In this section, the RF power handling will be discussed at 28 GHz (a frequency band of interest for 5G wireless networks). To assess in detail the linearity of the multi-PD photodiodes, IP3 (third order intercept point) measurements were used. In order to make sure that the measured non-linearities are caused by the DUT, the two-wavelength measurement setup discussed in [17] was implemented. The adopted setup can be seen in Fig. 9. This setup consists of two transmitters working at different wavelengths. It is important that both wavelengths are far enough from each to make sure that beat notes between the two cannot be received by the photodetector. On the other hand, the wavelengths should be close enough to the center wavelength (1550 nm) such that the optical components (e.g. star coupler) still work as expected. Therefore, the lasers were set to send a continuous wave signal at 1548 and 1552 nm. Both lasers are afterwards externally modulated with a sine wave which slightly deviates from the desired RF frequency. To this end, the 1548 and 1552 nm lasers were respectively modulated with a 27.999 GHz and 28.001 GHz sine by a LiNbO3 MZM biased at its quadrature point and driven at a 34 percent modulation depth. The modulated signals coming from both transmitters are subsequently combined, amplified with an EDFA and finally sent to the DUT. In the DUT, the two tones will be generated and these will in turn give rise to intermodulation products that are caused by the receiver rather than the whole link. Only the ESA and DUT will produce third order intermodulation products at 27.997 and 28.003 GHz. The optical components might generate beat products but the two optical

frequencies are spread by approximately 500 GHz (i.e. a spacing of 4 nm at 1550 nm) and therefore those optical non-linearities will not distort the obtained results. The modulator on the other hand can generate a signal at twice the fundamental frequency and this can cause overlapping beat products by mixing with the fundamental tone of the other transmitter. However, since the MZM is biased at its quadrature point, only odd order harmonics will be introduced and the output spectrum of the MZM will be reasonably free of even order harmonics. This will help to minimize intermodulation products caused by the second harmonic generated in one MZM and the fundamental tone generated in the other MZM. Consequently, the third-order intermodulation product of the DUT will be more accurately determined [17].

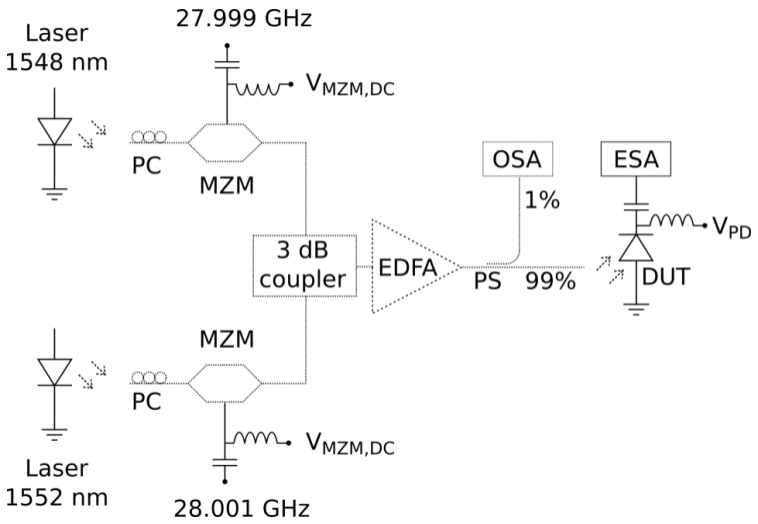


Fig. 9. Setup used for IP3 linearity measurements (OSA: Optical Spectrum Analyzer, ESA: Electrical Spectrum Analyzer).

Non-linearities induced by the ESA and DUT can be discriminated by measuring the intermodulation products for different attenuation settings of the ESA. The receiver can be presented as Fig. 10.

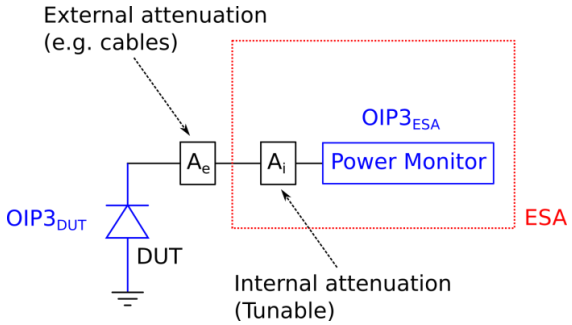


Fig. 10. IP3 contributions in the receiver chain.

The measured OIP3 (output referred third order intercept point) of the receiver chain will consist of two terms as shown in Eq. (5) [18].

$$\frac{1}{OIP3_{Rx}} = \frac{A_e A_i}{OIP3_{DUT}} + \frac{1}{OIP3_{ESA}} \tag{5}$$

Equation (5) shows that the OIP3 of the DUT can be found by making the internal attenuation of the ESA sufficiently high, such that the term depending on the linearity of the ESA can be neglected. The results of the OIP3 measurements (at 28 GHz) are provided in Table 2. One can see a 7 dB increase in power handling capabilities when dual feeding the PD. Additionally, it is clear that multi-PD structures are capable of handling higher powers. Adding multiple photodetectors in parallel results in RC low pass filtering as discussed before. Taking into account the frequency dependent current-to-power conversion, displayed in Fig. 4, of the parallel combination of 16 PDs, an improvement of approximately 9.5 dB over the dual fed, standalone germanium photodetector is expected. This value agrees reasonably well to the measured linearity improvement, namely 10.6 dB. For the TWPD with and without dummy termination improvements of respectively 14.2 dB and 14.6 dB are to be expected over the standalone, dual fed Ge PD based on Fig. 4. The measured improvements in linearity are respectively 15.8 dB and 13.2 dB. Simulations indicated that the slightly higher power handling capabilities at 28 GHz would be achieved without dummy termination while the measurements show that more power can be obtained by adding the termination resistor. A possible explanation for the discrepancy is a deviation in the equivalent network of the Ge PD.

**Table 2. Output referred third order intercept points at 28 GHz.**

| *Imec iSiPP25G, Silicon Photonics* | |
|---|---|
| Ge PD, Single fed | -1.79 dBm |
| Ge PD, Dual fed | 5.22 dBm |
| Lumped parallel configuration, 16 Ge PDs | 15.83 dBm |
| TWPD, 16 Ge PDs, without $R_{Term}$ | 18.43 dBm |
| TWPD, 16 Ge PDs, with $R_{Term}$ | 20.98 dBm |

## 5. Conclusion

Centralization is key in making future wireless network architectures feasible. Typical implementations of an ARoF link comprise of electrical amplification at the antenna. To push towards an increase in centralization and therefore a drop in cost and power consumption, amplification can be done for multiple RAUs simultaneously. Optical amplification at the CO will however require opto-electronic conversion with high power handling capabilities. In case of mmWave communication, a traveling wave photodiode with a monolithically integrated star coupler implemented on a silicon photonics platform is proposed in this paper. The TWPD combines high linearity with high bandwidth while the star coupler allows for a compact solution that preserves the high linearity obtained from adopting a multi-PD architecture. In this paper, a TWPD is described that has a 3 dB bandwidth of 27.5 GHz with a gentle roll-off off at higher frequencies allowing for mmWave operation. Additionally, the OIP3 of the TWPD is found to be nearly 21 dBm which is a significant improvement over the standard single fed Ge PD where the OIP3 is -1.8 dBm.

## Funding

Ghent University Special Research Fund (BOF14/GOA/034); European Research Council (695495); AFOSR (FA95501810015).

## References


1. J. G. Andrews, S. Buzzi, W. Choi, S. V. Hanly, A. Lozano, A. C. K. Soong, and J. C. Zhang, "What will 5G be?," IEEE J. Sel. Areas Commun. **32**(6), 1065–1082 (2014).
2. V. A. Thomas, M. El-Hajjar, and L. Hanzo, "Performance improvement and cost reduction techniques for radio over fiber communications," IEEE Commun. Surveys Tuts **17**(2), 627–670 (2015).
3. D. Novak, R. B. Waterhouse, A. Nirmalathas, C. Lim, P. A. Gamage, T. R. Clark, M. L. Dennis, and J. A. Nanzer, "Radio-over-fiber technologies for emerging wireless systems," IEEE J. Quantum Electron. **52**(1), (2016).
4. L. Bogaert, J. Lambrecht, A. Abbasi, J. Van Kerrebrouck, G. Torfs, X. Yin, G. Roelkens, and J. Bauwelinck, "Resonant optical receiver design by series inductive peaking for sub-6 GHz RoF," Wiley Microw. Opt. Technol. Lett. **59**(9), 2279-2284 (2017).
5. P. Liu, K. J. Williams, M. Y. Frankel, and R. D. Esman, "Saturation characteristics of fast photodetectors," IEEE Trans. Microw. Theory Techn. **47**(7), 1297–1303 (1999).
6. O. Caytan, L. Bogaert, H. Li, J. Van Kerrebrouck, S. Lemey, G. Torfs, J. Bauwelinck, P. Demeester, S. Agneessens, D. Vande Ginste, and H. Rogier, "Passive opto-antenna as downlink remote antenna unit for radio frequency over fiber," J. Lightwave Technol. **36**(19), (2018).
7. X. Xie, Q. Zhou, E. Norberg, M. Jacob-Mitos, Y. Chen, A. Ramaswamy, G. Fish, J. E. Bowers, J. Campbell, and A. Beling, "Heterogeneously integrated waveguide-coupled photodiodes on SOI with 12 dBm output power at 40 GHz," 2015 Optical Fiber Communications Conference and Exhibition (OFC), Los Angeles, CA (2015).
8. H. Pan, Z. Li, A. Beling, and J. Campbell, "Measurement and modeling of high-linearity modified uni traveling carrier photodiode with highly-doped absorber," Opt. Express **17**, 20221-20226 (2009).
9. T. Ohno, H. Fukano, Y. Muramoto, T. Ishibashi, T. Yoshimatsu, and Y. Doi, "Measurement of intermodulation distortion in a unitravelingcarrier refracting-facet photodiode and a p–i–n refracting-facet photodiode," IEEE Photon. Technol. Lett. **14**(3), 375–377 (2002).
10. M. Chtioui, D. Carpentier, B. Rousseau, F. Lelarge, A. Enard, and M. Achouche, "Experimental and theoretical linearity investigation of high-power unitraveling-carrier photodiodes," IEEE Photon. Technol. Lett. **21**(17), 1247–1249 (2009).
11. Z. Li, H. Pan, H. Chen, A. Beling, and J. C. Campbell, "High-saturation-current modified uni-traveling-carrier photodiode with cliff layer," IEEE J. Quantum Electron. **46**(5),626-632 (2010).
12. Andreas Beling, Allen S. Cross, Molly Piels, Jon Peters, Qiugui Zhou, John E. Bowers, and Joe C. Campbell, "InP-based waveguide photodiodes heterogeneously integrated on silicon-on-insulator for photonic microwave generation," Opt. Express **21**, 25901-25906 (2013)
13. G. Zhou, W. Ebert, S. Mutschall, A. Seeger, P. Runge, Q. Li, and A. Beling, "High-power waveguide integrated modified uni-traveling-carrier (UTC) photodiode with 5 dBm RF output power at 120 GHz," 2016 Optical Fiber Communications Conference and Exhibition (OFC), Anaheim, CA (2016).
14. C.-M. Chang, J. H. Sinsky, P. Dong, G. de Valicourt, and Y.-K. Chen, "High-power dual-fed traveling wave photodetector circuits in silicon photonics," Opt. Express **23**, 22857–66 (2015).
15. T. Spuesens, S. Pathak, M. Vanslembrouck, P. Dumon, and W. Bogaerts, "Grating couplers with an integrated power splitter for high-intensity optical power distribution," IEEE Photon. Technol. Lett. **28**(11), 1173–1176 (2016).
16. L. Y. Lin, M. C. Wu, T. Itoh, T. A. Vang, R. E. Muller, D. L. Sivco, and A. Y. Cho, "High-power high-speed photodetectors – design, analysis, and experimental demonstration," IEEE Trans. Microw. Theory Techn. **45**(8), 1320–1331 (1997).
17. H. Jiang, D. S. Shin, G. L. Li, T. A. Vang, D. C. Scott, and P. K. L. Yu, "The frequency behavior of the third-order intercept point in a waveguide photodiode," IEEE Photon. Technol. Lett. **12**(5), 540–542 (2000).
18. B. Razavi, *RF microelectronics* (Prentice Hall, 2011), 2nd ed., Chapter 2.